Journal of Magnetism and Magnetic Materials 474 (2019) 643–653

Contents lists available at ScienceDirect

Journal of Magnetism and Magnetic Materials

journal homepage: www.elsevier.com/locate/jmmm

Research articles

Neutron grating interferometry investigation of punching-related local magnetic property deteriorations in electrical steels

H.A. Weiss[a,*], S. Steentjes[b], P. Tröber[a], N. Leuning[b], T. Neuwirth[c], M. Schulz[c], K. Hameyer[b], R. Golle[a], W. Volk[a]

[a] Technical University of Munich, Chair of Metal Forming and Casting, Garching, Germany
[b] RWTH Aachen University, Institute of Electrical Machines, Aachen, Germany
[c] Technical University of Munich, Heinz Maier-Leibnitz Zentrum, Garching, Germany

ARTICLE INFO

Keywords:
Punching
Shear cutting
Residual stress
Non-oriented electrical steel
Magnetic property degradation
Neutron grating interferometry

ABSTRACT

Mechanical residual stress induced by manufacturing influences the magnetic behavior of non-grain oriented electrical steels, which are used for producing rotors and stators of electrical machines. The impairment occurs mainly along the cutting line of stator and rotor laminations. A locally resolved assessment of the magnetic material behavior of punched electrical steels is possible by using the neutron grating interferometry. In addition to this in situ measurement method, additional ex-situ measurements allow correlating local domain wall mobility and global magnetic polarization. Four different non-grain oriented electrical steels are investigated in this paper. This includes two sheet thicknesses of 0.35 mm and 0.65 mm both available having silicon contents of 2.30 wt-% as well as 2.74 wt-%. The specimens are produced by wire cutting and by punching using different process parameters, i.e., two relative cutting clearances of 5% and 10% plus a sharp and worn cutting edge wear state. The cutting method's influence on the four different electrical steel's magnetic behavior is discussed with respect to the local polarization distributions at varying magnetic field strengths next to the cutting lines. This novel approach for the first time allows an in situ investigation of altered magnetic properties with respect to the punching induced residual stress along the cutting line. Not only the maximum deterioration of the polarization next to the cutting line but also the extent of the magnetic property deterioration is pointed out. The effect of punching parameter variations is further verified using global magnetic measurements. The knowledge about the local polarization distribution next to the cutting line is critical for an improved development and design of electrical machines.

1. Introduction

When developing and designing efficient electrical machines, a detailed knowledge of the magnetic material behavior of the built-in components is crucial. Manufacturing non-grain oriented electrical steels to stacked rotor and stator cores of electrical machines has a negative effect on the resulting magnetic material properties. It is common to use building factors, to take deteriorated magnetic material properties into account [1]. Since they not only depend on the actual influence of the manufacturing process itself but also on the rotor and stator setup that has been used for determining them, electromagnetic components often have a different magnetic behavior than assumed. A detailed knowledge of the punching influence helps to improve the building factors, to reduce costly oversizing and to increase an electric drive's energy efficiency.

Punching the desired lamination geometries from the electrical steel leads to plastic deformations next to the cutting line. These deformations induce mechanical tensions and compressive residual stress, which inhibit the domain wall mobility and, therefore, affect the overall magnetic behavior [2,3]. Especially, varying punching parameters can influence induced residual stress and, therefore, specific iron loss and magnetic field strength to reach a certain magnetic polarization [4]. One of these punching parameters is the cutting edge wear state, which directly correlates to the total number of parts that have been cut. Fig. 1 depicts the impact of the cutting edge wear state on the resulting residual stress as well as on the resulting microhardness increase next to the cutting surface. A non-grain oriented electrical steel with 2.4 wt-% silicon and a thickness of 0.5 mm was punched with sharp and blunt cutting edges. The blunt cutting edges were polished to a radius of 70 μm. The horizontal distance between the two cutting edges, the

* Corresponding author.
E-mail address: hw@utg.de (H.A. Weiss).

https://doi.org/10.1016/j.jmmm.2018.10.098
Received 12 June 2018; Received in revised form 11 September 2018; Accepted 19 October 2018
Available online 22 October 2018

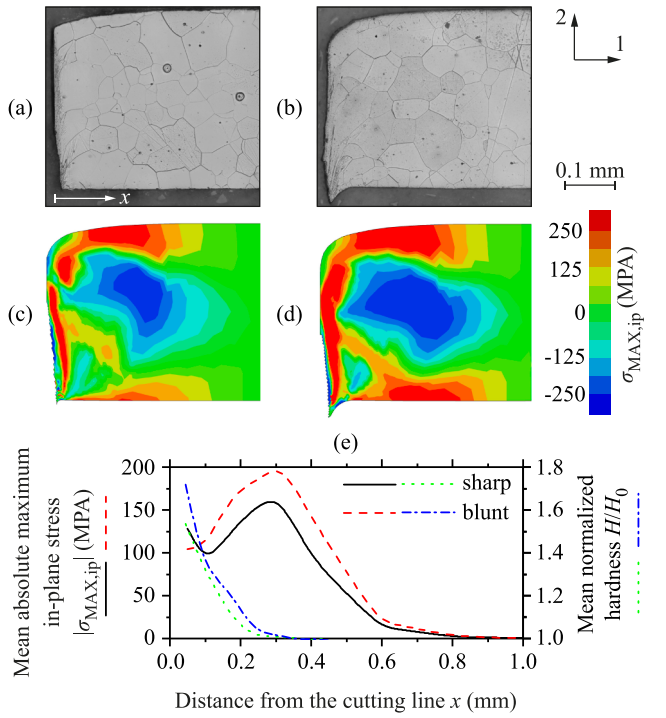

Fig. 1. Micrographs and residual stress distribution of an electrical steel with 0.5 mm thickness and a silicon content of 2.4 wt-% manufactured with an industrial punching tool that has a cutting clearance of 35 μm and two different cutting edge wear states; (a), (c) sharp cutting edges; (b), (d) blunt cutting edges; (e) distribution of mean normalized hardness and the mean absolute maximum in-plane stress over the distance to the cutting line x.

cutting clearance, was set to 35 μm. Micrographs and a residual stress plot of a numerical punching analysis are shown in Fig. 1 for an electrical steel cut with (a), (c) sharp and (b), (d) worn cutting edges. The increased amount of plastic deformation when cutting with a blunt tool can be easily seen in the micrographs and the residual stress distributions. A comparison of the mean residual stress and the mean normalized hardness plotted against the distance to the cutting surface is depicted in Fig. 1 (e). Blunt cutting edges lead to an increased material hardening across a bigger area and larger residual stress with deeper penetration than sharp cutting edges. It can be noticed, that the residual-stress-affected area reaches up to three times the depth of the area affected by plastic deformation into the material. Increasing the cutting clearance also results in higher residual stress and material hardening next to the cutting line [5].

The relation of residual stress and reduced domain wall mobility is known as the inverse magnetostrictive effect [6]. The extent of a magnetic property deterioration due to induced mechanical stress largely depends on the stress amplitude and algebraic sign [7]. In addition, the influence on the magnetic material properties varies with it's orientation to rolling direction (RD) and the material's grain size [8,9].

The magnetic deterioration in the area near the cut edge includes a decrease of permeability, an increase of both static and dynamic hysteresis loss, as well as a degradation of magnetization. These effects are restricted to the area bordering the cut edge and, therefore, alter the material locally. In FE machine simulation, the magnetic material properties are generally incorporated in the form of a local loss model and magnetization curves, parametrized by standardized measurements. However, the effect of material degradations due to cut edges on the local flux density distribution and related local and total iron losses has to be accounted for to improve the accuracy of FE simulations. The authors of [10] show that although the torque and active power of the machine are not primarily affected by cutting, the iron loss increased over 35% for an exemplary 37 kW induction motor modeled with regard to the cutting edge effects. Different models to describe the changing local magnetization and loss behavior due to cutting have been published [11]. Nevertheless, an accurate modeling of the local polarization requires further knowledge on the actual effect of mechanical stress on the local magnetic properties, i.e., domain wall configurations and frequency behavior.

Frequently, magnetic properties of electrical steels and, in particular, the influence of the cutting process are analyzed by using a standardized single-sheet test (SST). This test method allows to examine the increase in specific loss and maximum magnetic field strength to reach a certain magnetic polarization with respect to an increasing cutting line length. An investigation of the punching influence on the magnetic material behavior for various non-grain oriented electrical steels proved that cutting related losses become smaller for increasing excitation frequencies, higher magnetic polarizations, less cutting edge wear and reduced cutting clearances [12]. Although a qualitative correlation between induced stress and global measured magnetic properties is obvious, a spatial quantification of the magnetically deteriorated area from a numerical determined residual stress distribution cannot be derived. This is due to the impact of a three-dimensional stress state, compared to the effect of a two-dimensional stress state, on the magnetic material behavior is not fully investigated yet [13,14].

In order to determine the extent of the local magnetic material degradation, spatially resolved instead of averaging global magnetic measurement methods are necessary. This not only allows the magnetically degraded area to be taken into account within the numerical evaluation of electric machines, but such measurements can also improve approaches that derive the degraded area from global magnetic measurement methods [15–17].

Analyzing local magnetic properties next to cutting surfaces is possible with a wide variety of methods. In [18,19] the cutting influence was investigated for the non-grain oriented electrical steel M250-35A using small search coils next to the cutting line. Using this method, a residual stress penetration depth of up to 12.5 mm was measured. It can be noticed that the size of the degraded area depends on the applied field strength. Magneto-optical Kerr effect analysis of punched cutting surfaces in [20] showed a penetration depth of 100–250 μm for a 0.35 mm thick electrical steel with 2.8 wt-% silicon. In [21] a residual stress penetration depth of 0.5 mm after cutting the electrical steel grade M470-50A was measured using nanoindentation. In addition, a magnetic domain structure analysis with the Bitter method revealed a residual stress-related domain structure change within the range of 0.3 mm to the cutting surface. A drawback of the aforementioned methods is their destructive nature. Specimens have to be prepared by grinding and polishing, which sets free mechanical residual stress and, therefore, changes the overall stress state. The limitation of the mentioned methods to only detect near-surface magnetic properties is another problem.

In [22] a synchrotron radiation diffraction method to analyze local resolved stress in a punched electrical steel sample is introduced. Although the measurement volume is not specified, it is possible to show that the elastic lattice strains reach up to 1 mm deep into the material. The strain distribution is in good accordance with the numerical cutting stress distribution shown in [5]. However, a correlation with local magnetic properties is still missing.

Neutron grating interferometry (nGI) is a novel measurement method that allows for a non-destructive, spatially resolved analysis of bulk magnetic material behavior [23,24]. Because of the high lateral resolution, the impact of different cutting processes on the local domain wall configuration next to the cutting line can be examined [25]. It is shown that the affected area has an extent of over five millimeters perpendicular to the cutting line. Similar nGI measurements in [26] exhibit a residual stress-affected area for a punched non-grain oriented electrical steel with a width of approximately 0.75 mm. However, punching parameters were not mentioned both times. A correlation of the measured results with a global magnetic measurement was in good

accordance in terms of the overall magnetic property deviation due to the separation process [27]. It was also possible to verify the interaction between external applied stress and magnetic material behavior using nGI in [28]. Despite the good capability of the measurement method to analyze punching-related magnetic property deteriorations, integrating magnetic properties over the material thickness is a small drawback. Since the consideration of local magnetic properties within the numerical magnetic design of electrical machines is based on such integrated data, a time-consuming three-dimensional tomographic investigation of the domain wall configuration, as conducted in [29], is not necessary.

Due to the good suitability of nGI to analyze the local magnetic behavior next to the cutting surface, it is used within this work. The impact of different punching parameters is investigated for four different non-grain oriented electrical steels. Both the size of the magnetically affected area, i.e., the residual stress penetration depth, as well as the local magnetizability depending on the distance to the cutting surface, are examined. The aim is a quantitative evaluation of the influence of punching on magnetic properties in order to develop and design more efficient electric machines.

2. Experimental setup

2.1. Sampling

In order to enable the transferability of the investigations to a wide range of possible applications, four industrial non-grain oriented electrical steels are selected. Four sample materials $A_{0.65}$, $A_{0.35}$, $B_{0.65}$ and $B_{0.35}$ are investigated consisting of two different alloys with a silicon content of 2.30 wt-% and 2.75 wt-%. Each grade is available with a sheet thickness s_0 of 0.35 mm and 0.65 mm, respectively. The results of a chemical composition analysis by using a spark spectrometer are shown in Table 1.

The different chemical compositions as well as the different rolling and heat treatment strategies of the four electrical steels lead to different metallographic, mechanical and magnetical properties listed in Table 2. The average grain size d_g is determined by using the line section method according to EN ISO 643. Yield strength *YS*, ultimate tensile strength *UTS* and uniform elongation A_g are measured according to EN ISO 6892-1 by using a tensile test setup. For the magnetic characterization of the specific iron loss P_S and the magnetic polarization J a 60 mm × 60 mm SST setup is used. The measurements are carried out according to EN 10106.

The specimens for the nGI investigations are produced by using a high-precision industrial punching tool operated at 100 strokes per minute with a mechanical single action press, which is industrially used to manufacture rotor and stator cores [12]. The precise punching tool enables small constant cutting clearances (CCL) down to 7 µm to be realized. In addition, the tool ensures a homogenous material deformation along the cutting line of the produced specimen. The dimensions of the specimen are 62 mm × 10 mm. In order to investigate different residual stress extents next to the cutting surface, four different parameter sets listed in Table 3 are used for punching.

By using absolute CCLs of 19 µm, 35 µm and 70 µm, a relative CCL of 5% and 10% relative to the sheet thickness for each electrical steel can be ensured. For each CCL, sharp cutting edges (CE) on the die and punch are available. In addition, a punch and die with worn CEs for a CCL of 35 µm is available. The CEs were machined in such a way that they show the same geometry as CEs that have already cut four million parts out of the non-grain oriented electrical steel grade NO 30-16. Since the qualitative influence of a punching parameter variation on the magnetic property deterioration is independent from the alignment of the cutting line to the rolling direction, all specimens have a cutting direction (CD) oriented perpendicular to rolling direction [12].

In addition to the punched specimens, wire-cut reference specimens have been produced perpendicular to and in rolling direction. Due to the gentle material removal, only small amounts of residual stress are induced during the cutting process. Therefore, a minimal magnetic property deterioration in the vicinity of the cutting line compared to a punched specimen can be assured [1].

Table 1
Chemical composition.

Material grade	Alloying element in wt-%				
	Si	Al	Mn	Other	Fe
A	2.30	1.19	0.27	< 0.05	Bal.
B	2.74	> 1.29	0.62	< 0.05	Bal.

Table 2
Mechanical and magnetic material properties.

Material		$A_{0.65}$	$B_{0.65}$	$A_{0.35}$	$B_{0.35}$
Material grade		A	B	A	B
Sheet thickness s_0 in mm		0.65	0.65	0.35	0.35
Grain size d_g in µm		102	121	70	87
Yield strength *YS* in MPa		376	472	400	494
Ultimate tensile strength *UTS* in MPa		513	589	527	613
Uniform elongation A_g in %		11.1	9.3	11.0	9.1
Specific loss P_S in W/kg at 50 Hz	1.0 T	1.78	1.64	1.42	1.30
	1.5 T	4.08	3.65	3.31	2.93
Magnetic polarization J in T at 50 Hz	2500 A/m	1.58	1.57	1.55	1.55
	5500 A/m	1.66	1.65	1.63	1.63

Table 3
Investigated punching parameter combinations.

Punching set	1	2	3	4
CCL in µm	19	35	70	35
$CCL_{0.65}$ in %	–	5.4	10.8	5.4
$CCL_{0.35}$ in %	5.4	10.0	–	10.0
CE wear state	Sharp	Sharp	Sharp	Worn

2.2. Neutron grating interferometry

nGI allows to simultaneously access information about attenuation, phase shift and the ultra-small-angle scattering of neutrons (USANS) in a sample. The information is calculated from images that are called transmission image (TI), differential phase contrast image (DPCI) and dark-field image (DFI) [30]. For the investigation of the punching influence, the DFI is of high interest, as it allows to spatially map the amount and size of magnetic domains, due to the scattering of neutrons on the walls of magnetic domains.

A neutron grating interferometer is an adaptation of an optical Talbot-Lau interferometer and consists of three line gratings [31]. Two absorption gratings (G_0 and G_2, period $p_0 \sim mm$ and $p_2 \sim$ µm) and one phase grating (G_1, $p_1 \sim 2p_2$), which are placed inside an existing neutron imaging beamline. In Fig. 2 a sketch of this concept is shown. Grating G_0 generates an array of coherent line sources, which are incoherent to each other. Downstream, the neutron beam n is split up by introducing a periodic phase modulation of π in the neutron wavefront. The split is mainly into the first orders while the zeroth order is suppressed [32]. This results in a complex intensity and phase modulation behind G_1, called Talbot carpet [33]. At certain distances behind G_1, the intensity modulation reaches a maximum. These distances are called fractional Talbot distances. Due to the π-phase shift, the periodicity of the resulting interference pattern is half the period of G_1. To be able to analyze this pattern, the second absorption grating is needed, as the period is too small to resolve with standard neutron detectors [34]. The

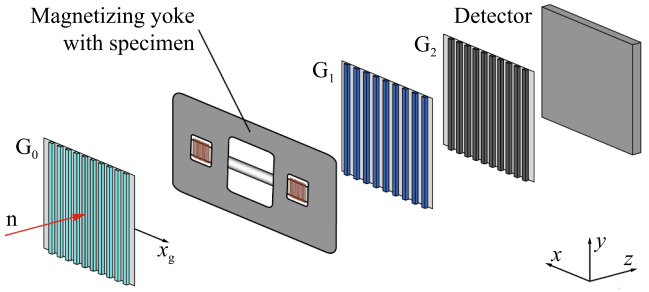

Fig. 2. Neutron grating interferometry setup.

G_2 grating is placed at a fractional Talbot distance. One of the gratings, in this case G_0, is moved perpendicular to the grating lines, to access the interference pattern.

The intensity oscillation I in every pixel (i,j) of the detector resulting from the grating shifts x_g can be approximated by

$$I(x_g, i, j) = a_0(i, j) + a_1(i, j)cos\left[\frac{2\pi x_g}{p_2} + \phi(i, j)\right], \tag{1}$$

with the intensity oscillation's offset a_0, amplitude a_1 and phase ϕ [23,35]. During one nGI scan at different positions x_g of grating G_0 an intensity modulation in each detector pixel can be measured. The acquired intensity values can be used to determine a_0, a_1 and ϕ with a Fourier transformation according to [36] or with a least-square approach as suggested in [37]. Performing this parameteridentification with (s) and without a sample (f) allows for the transmission image (TI) and the dark field image (DFI) to be calculated as follows [23,35]:

$$\mathrm{TI}(i, j) = \frac{a_0^s(i, j)}{a_0^f(i, j)}, \tag{2}$$

$$\mathrm{DFI}(i, j) = \frac{a_1^s(i, j)a_0^f(i, j)}{a_0^s(i, j)a_1^f(i, j)}. \tag{3}$$

The mechanisms responsible for the above mentioned modulation can be accounted to neutron absorption, refraction and scattering. Exemplarily the absorption and scattering mechanisms are depicted in Fig. 3. While the TI only displays the attenuation of the interference pattern in (a) the DFI visualizes scattering of neutrons under ultra-small angles (b). Since the interaction of the neutron's magnetic moment with areas having varying magnetic refraction indices, i.e., different oriented magnetic domains separated by domain walls, results in such small angle neutron scattering, the DFI contrast according to 3 can be used to analyze the materials local magnetic behavior [38].

For the experiment performed, the nGI-setup of the ANTARES imaging beamline at the FRM II has been used [35,39,40]. The measurements were performed at a neutron wavelength of 3.2 Å. For each nGI-scan the G_0 grating was moved to ten equidistant positions over one period of G_0. At each position three images were taken, each with an exposure time of 20 s. This resulted in a total exposure time of 600 s per image. The used field of view was 57.6 mm × 68.2 mm with a pixel size of 27 m. The used scintillator screen had a thickness of 100 µm. The evaluation area was set to 51.8 mm × 22.4 mm. For each processed electrical steel specimen, nGI-scans were performed with different magnetic fields applied to analyze the reaction of the DFI-signal on the magnetization.

2.3. Specimen magnetization

Specimen magnetization is performed using a yoke that has a flat design to decrease the distance between specimen and grating G_1. The magnetization yoke is built up from stacked non-grain oriented electrical steel laminations out of the material grade M300-35A. The three-legged yoke structure ensures a homogeneous magnetic field

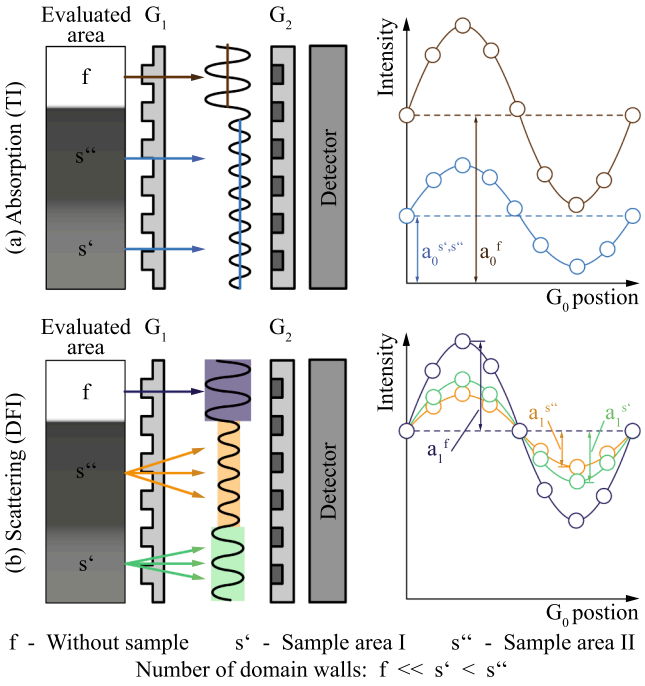

Fig. 3. Two nGI contrast mechanisms (a), absorbtion and (b), scattering that influence the intensity oscillation at the detector during one nGI scan.

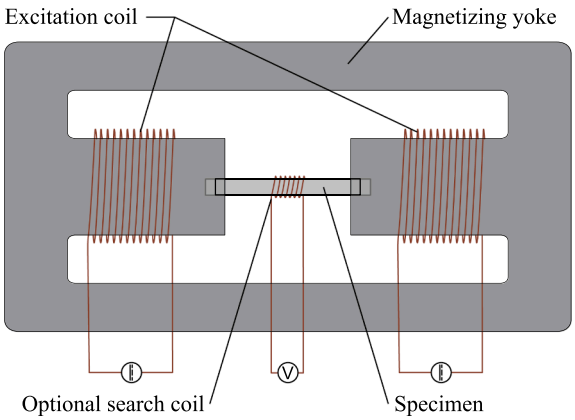

Fig. 4. Specimen magnetization setup.

distribution within the sample. Two copper excitation coils with 75 windings and a length of 45 mm are used to magnetize yoke and specimen. Fig. 4 displays the magnetizing yoke.

Before each measurement, the specimens were demagnetized within the yoke. The impact of the punching process on the magnetic material behavior is analyzed for static magnetic fields. The lower the excitation frequency is, the lower is the impact of the residual stress on the domain wall mobility and, therefore, the overall magnetic material properties [12]. Measurements using nGI are carried out for eight different currents I, respectively, magnetic field strengths H shown in Table 4. For material B, no nGI tests for a magnetic field strength of 11,120 A/m are carried out, since the field strength for this series was not included in the measuring program.

Besides the in situ nGI analysis, additionally an ex-situ measurement

Table 4
Investigated current I and magnetic field strength H

Current I in A	0.00	0.13	0.27	0.47	1.34	2.00	5.00	6.67
Field strength H in A/m	0	220	450	780	2,230	3,330	8,330	11,120

of the magnetic properties is performed. Using an optional search coil with 50 windings and a length of 30 mm, the magnetic polarization J of the wire-cut specimens is measured by using a computer assisted setup according to the international standard IEC 60404-3. This allows comparing local nGI data with global specimen polarization for different magnetic field strengths.

3. Results and discussion

In order to investigate the punching impact on the local magnetizability, a detailed knowledge regarding the correlation of dark field image contrast and polarization is necessary. Since the dark field image contrast obtained by using nGI is directly associated with the number of domain walls present over the specimen thickness, altered magnetic properties due to punching induced stress in the area next to the cutting line can be observed. First, the extent of punching on the DFI contrast is analyzed at different magnetic field strengths. Second, the sensitivity of the DFI contrast to cutting line orientation, sheet thickness and silicon content variations is shown. Third, utilizing the optional search coil, local polarizations can be calculated from the DFI contrasts, allowing the punching impact to be studied.

3.1. nGI evaluation method

Bulk magnetic material properties are examined using the dark field images (DFI) calculated from the nGI measurements. For each specimen and field strength, the local magnetic domain wall state is available as a two-dimensional dark field contrast image. Fig. 5 shows two such images. In (a) a wire-cut specimen and in (b) a punched specimen out of material $A_{0.35}$ are shown for a magnetic field strength of 750 A/m. The punched specimen is processed with punching parameter set (PS) two. The investigated horizontal cutting line has an orientation of 90° to rolling direction. Within the images, a contrast of one is synonymous with no neutron beam scattering, whereas a contrast value of zero implies excessive neutron beam scattering. Comparing the punched to the wire-cut specimen, a small area along the punched edges with a decreased DFI contrast can be observed. Obviously neutron beam scattering and thereby DFI contrast is increased within the area next to the cutting line, because of an increased domain wall density. This results from the magnetically anisotropic material behavior. Punching changes the local stress state, leads to grain refinement and induces dislocations in the vicinity of the cutting line. As a consequence, the local domain configuration is deteriorated [26,27].

By investigating the DFI contrast C_{DFI} distribution over the specimen width, a quantitative evaluation of the local domain wall configuration and thereby the local magnetic state is possible. In Fig. 5 the dashed boxes indicate the evaluation range in which the DFI contrast profile is calculated. Averaging the DFI contrast profile over a horizontal distance of 900 pixel, respectively, 24.3 mm assures statistically significant results. Fig. 6 displays the DFI contrast profiles of the wire-cut and

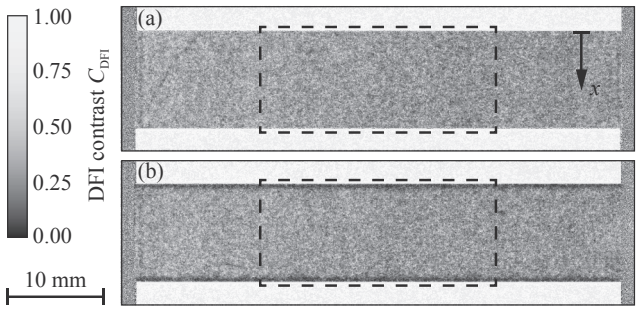

Fig. 5. Dark field contrast image for a wire-cut (a) and a specimen punched with parameter set 2 (b) out of material $A_{0.35}$ for a magnetic field strength of 780 A/m.

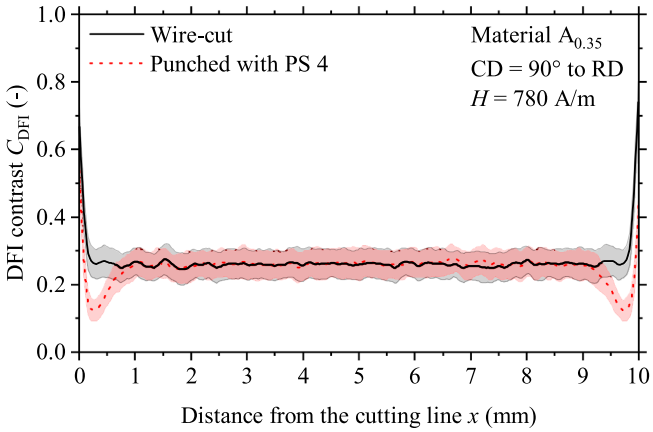

Fig. 6. DFI contrast C_{DFI} plot over the distance from the cutting line x for a wire-cut and punched (PS 4) specimen out of material $A_{0.35}$ magnetized 90° to RD at a magnetic field strength of 780 A/m.

punched specimens discussed above as well as their standard deviations. While the contrast profile of the wire-cut specimen is homogenous over the specimen width, the DFI contrast profile of the punched specimen has a local minimum next to the cutting line. Comparing the punched DFI contrast profile with the stress profile of Fig. 1, a similar local maximum can be found within the same area next to the cutting line. With increasing distance, the contrast profile of the punched specimen approximates the profile of the wire-cut specimen. It is apparent that the manufacturing method used has a significant influence on the local domain wall configuration and thus on the global magnetization of the specimen.

In the area within 100 μm next to the cutting line, a strong increase of the DFI contrast can be noticed even when looking at the wire-cut specimens. On the one hand, this increase can result from a signal blurring at the scintillator within two to three pixels of the cutting line. On the other hand, the local DFI contrast acquired by nGI depends on the domain orientation [23]. Since domains with a different alignment are present next to the cutting line, a DFI contrast rise can also originate from this change in domain orientation.

Changing the applied field strength results in a variation of the domain wall configuration and, therefore, in an alternating overall specimen magnetization. Increasing domain wall motion due to the higher external magnetic field provokes domain growth and reorientation within the specimen. This variation of the magnetic domain configuration leads to less neutron scattering because of a smaller number of magnetic domain walls. As a consequence, the DFI contrast increases for higher field strength values. This is depicted in Fig. 7 for a

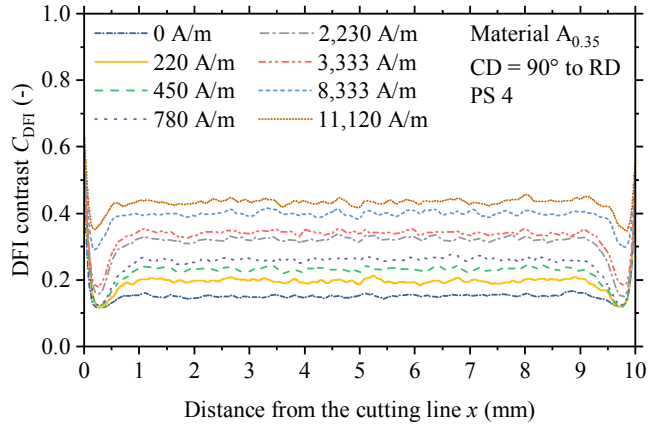

Fig. 7. Impact of a field strength variation on the DFI contrast profile of a specimen punched with PS 4 in 90° to rolling direction out of material $A_{0.35}$.

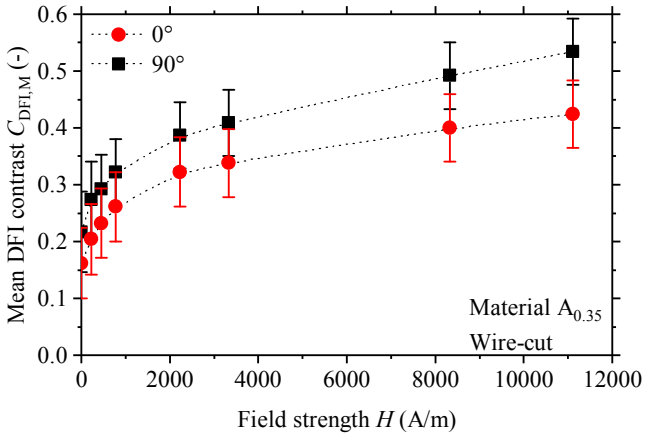

Fig. 8. Mean DFI contrast $C_{DFI,M}$ plot over the magnetic field strength H for specimens wire-cut out of material $A_{0.35}$ and magnetized 0° and 90° to rolling direction.

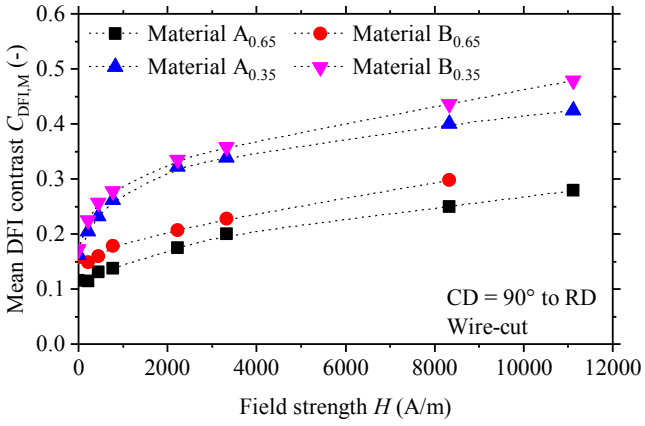

Fig. 9. Silicon content and sheet thickness impact on the mean DFI contrast $C_{DFI,M}$ at various magnetic field strengths H using wire-cut specimens magnetized 90° to rolling direction.

specimen punched with punching set 4 perpendicular to rolling direction out of material $A_{0.35}$. Since low stress affects the magnetic properties by a smaller amount than high stress, residual stress-affected areas within the vicinity of the cutting line tend to become smaller for higher field strength values.

3.2. Rolling direction influence on the DFI contrast

Non-grain oriented electrical steels have an anisotropic magneto-crystalline texture. Due to this, the overall domain density distribution is also anisotropic. This results in non-uniformly distributed global magnetic properties. A nGI measurement of wire-cut specimens for each material confirms this behavior. In Fig. 8 this is exemplarily shown for material $A_{0.35}$. Within the plot mean DFI contrast $C_{DFI,M}$ over magnetic field strength is depicted for a cutting line alignment in and perpendicular to rolling direction. Thereby, the mean DFI contrast is calculated over the whole specimen width. The plot confirms global measurements showing an anisotropic magnetic material behavior. Independent of the magnetic field strength, the mean DFI contrast of specimens magnetized in rolling direction is always higher than the mean DFI contrast of specimens magnetized perpendicular to the rolling direction. In addition, the gradient with which the mean DFI contrast increases is also dependent on the rolling direction and is always higher for specimens magnetized in rolling direction.

3.3. Grain size and sheet thickness influence

A comparison of mean DFI contrast over magnetic field strength for the investigated materials in Fig. 9 shows the influence of the silicon content and sheet thickness. The specimens are wire-cut and magnetized along rolling direction.

Smaller sheet thickness for a constant silicon content results in an increased mean DFI contrast independent of the investigated magnetic field strength. Hereby, the smaller number of domain walls leads to a decreasing number of scattered neutrons.

Alternating the material grade from a low silicon content to a higher one increases the grain size and therefore decreases the number of magnetic domains, respectively, magnetic domain walls [41]. This leads to less neutron scattering at a constant sheet thickness. In addition to that, the mean DFI contrast gradient also rises.

3.4. Magnetizing frame calibration

In order to investigate the influence of punching on the local magnetic material behavior, the local polarization, with respect to the distance from the cutting line, has to be calculated from the DFI contrast plots. Converting the DFI contrast to a local polarization value is made possible by comparing the mean DFI contrast at distinct field strengths with the commutation curves of the material. To acquire the commutation curves, the magnetizing frame is used. With the aid of a computer-assisted measurement setup, a sinusoidal signal with a frequency of 50 Hz is applied to the excitation coil to magnetize a wire-cut specimen of each material grade. By using the optional search coil, the maximum magnetic polarization J_{max} is measured. The measurements are carried out for polarization values in between 0.3 T and 1.5 T in steps of 0.1 T. Polarization values beyond 1.5 T are calculated using the Fröhlich-Kennelly extrapolation according to [6]. Since only the maximum polarization is of interest, measuring at lower excitation frequencies than 50 Hz provides similar results. A good signal quality is assured by calculating the form factor for each measured value. Fig. 10 shows the commutation curves for the four different materials with a cutting line oriented perpendicular to the rolling direction.

Combining globally measured maximum polarization (Fig. 10) with local measured mean DFI contrast (Fig. 9) at the same magnetic field strengths allows to calculate the local resolved polarization from the nGI measurement. To get the values of global polarization and local DFI contrast at the same magnetic field strengths, both curves (Fig. 9 and Fig. 10) were linearly interpolated in between 0 A/m and 12,000 A/m at 200 equally distributed values. The resulting maximum polarization over mean DFI contrast plot is displayed in Fig. 11 for the four materials wire-cut perpendicular to rolling direction.

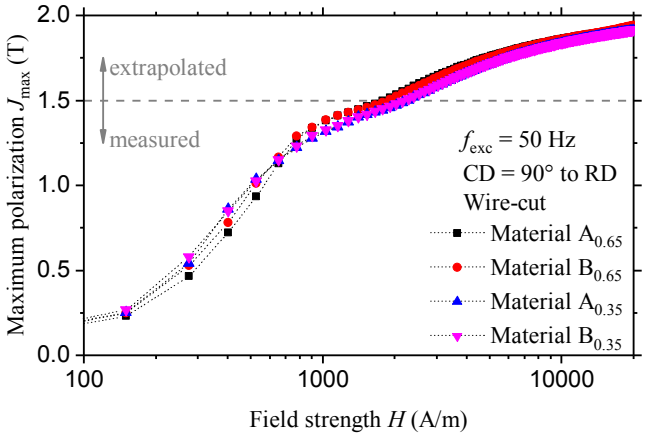

Fig. 10. Maximum polarization J_{max} over field strength H for wire-cut specimens of each material grade with a cutting line oriented in 90° to rolling direction at an excitation frequency of 50 Hz.

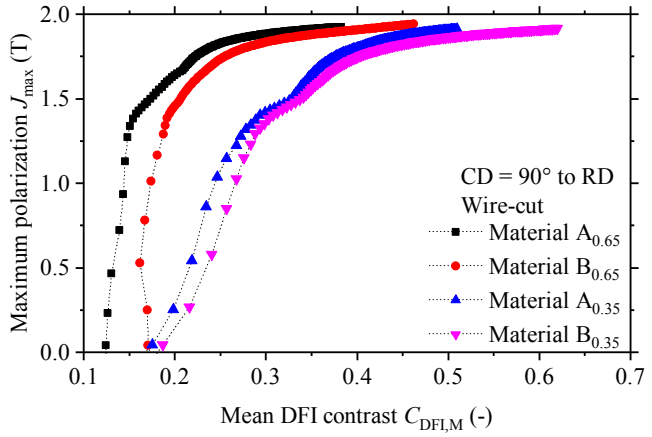

Fig. 11. Maximum Polarization J_{max} over mean DFI contrast $C_{DFI,M}$ curves of material $A_{0.65}$, $A_{0.35}$, $B_{0.65}$ and $B_{0.35}$ wire-cut 90° to rolling direction.

Calculating the local polarization from the local DFI contrast is possible by different approaches. As already shown in [25,27], a conversion can be done using an exponential fit. Doing so, a coefficient of determination above 0.95 can be reached. Nevertheless, the curves in Fig. 11 indicate that the correlation is affected by different sheet thicknesses and silicon contents. Especially the silicon content changes the grain size as well as the mean magnetic domain size. This affects the number of domain walls moved when alternating the magnetic field. Since the relation in between the number of moved domain walls over sheet thickness and the global magnetic polarization is not clear, the local magnetic polarization J_{local} is calculated from the DFI contrast by using the curves in Fig. 11 as a mapping database. For each material, the mapping database of a wire-cut specimen is used, as the maximum polarization over DFI contrast curve is independent of the manufacturing method [25].

By calculating the local magnetic polarization curves, a detailed investigation of punching-related magnetic property deteriorations in the vicinity of the cutting line is made possible. However, also a mapping based approach has a downside. In comparison to the maximum polarization over mean DFI contrast curves of material $A_{0.35}$ and $B_{0.35}$, the curves of $A_{0.65}$ and $B_{0.65}$ show a strong slope beyond polarization values of 1.25 T. These strong slopes result in huge polarization fluctuations for little DFI contrast variations. In addition to this problem, a clear allocation of local DFI to local polarization values at low magnetic field strengths cannot be made for material $A_{0.65}$ and $B_{0.65}$, since a small decrease of the mean DFI contrast for field strengths below 500 A/m for material $A_{0.65}$ and 1000 A/m for $B_{0.65}$ in Fig. 9 can lead to an unclear local polarization assignment when using the mapping databasis. Due to these two problems, a calculation of local polarization curves for material $A_{0.65}$ and $B_{0.65}$ is only carried out for field strengths above 780 A/m and 1000 A/m, respectively.

3.5. Effect of the punching process on local magnetic properties

The influence of different punching parameters on the magnetic properties of material $A_{0.65}$, $B_{0.65}$, $A_{0.35}$ and $B_{0.35}$ with respect to varying magnetic field strengths is investigated in a two-millimeter-wide area adjacent to the cutting line using the mapping database in Fig. 11. For the investigation, the cutting line is oriented perpendicular to the rolling direction. The mapped local polarization curves are shown in Fig. 12.

Induced stress and deformations can lead to domain refinement and domain wall pinning. These effects change the average domain configuration over sheet thickness. Since the approach using a mapping database does not provide polarization values for very small DFI contrasts, the local polarization values for lower DFI contrasts are linearly extrapolated. Negative polarization values that might emerge from this extrapolation are considered incorrect and are therefore not displayed within Fig. 12.

Independent of material and punching parameters used, a variation of the punching-affected area for different magnetic field strengths can be observed. Increasing the field strength reduces this area. For high magnetic field strength values, even the orientation of the domains directly adjacent to the cutting line changes. The result is a nearly homogeneous local magnetic polarization across the whole specimen width.

The extent of punching-related local magnetic property deteriorations is directly related to the microhardness and residual stress profile in Fig. 1. Remembering that tension and pressure stress as well as their magnitude have a different impact on the magnetic properties helps understanding the local magnetic polarization curves. Areas that are not saturated at high magnetic field strengths lie within a distance of 0.2 mm–0.4 mm next to the cutting line. Here, also the maximum absolute stress shows a local maximum. This behavior goes along with the magneto-elastic analysis in [2,8,9], which proves that high stress has a bigger impact on the magnetic properties than small stress.

Compared to the stress influence, the impact of plastic deformations is small. High plastic deformations directly adjacent to the cutting line lead to grain refinement and domain wall pinning. This only affects the domain wall motion at low and medium magnetic field strengths [27]. In contrast, induced stress affects the overall magnetic material behavior.

The resulting local magnetic polarization curves are further discussed regarding the influence of the sheet thickness, silicon content, cutting clearance and cutting edge wear state.

3.5.1. Sheet thickness

The results show a significant influence of the sheet thickness regardless of silicon content, punching parameters and field strength. Due to the larger material volume that gets deformed during punching, the area affected by residual stress is increased and reaches further into the material [5]. Changing the thickness from 0.35 mm to 0.65 mm results in an affected area that nearly doubles its extension from the cutting line. In addition, the level of polarization within the local minimum is also decreased.

3.5.2. Silicon content

For constant sheet thicknesses, an increased area that is deteriorated due to punching can be noticed for higher alloyed electrical steels. A higher silicon content significantly raises the yield strength, ultimate tensile strength and grain size, while the uniform elongation is slightly decreased. Smaller uniform elongations result in a faster material failure and therefore a smaller plastically deformed area. Nevertheless, a larger yield strength and ultimate tensile strength allow for higher stress to be present within an electrical steel. Further, if the grain size is at least within the scale of the cutting clearance, the cutting force increases for rising grain sizes [42,43].

3.5.3. Cutting clearance

Generally, small clearances should be preferred over large clearances. Especially when manufacturing thicker electrical steels, a clear influence of the cutting clearance is observable. High clearances lead to an increased material deformation due to the larger gap in between the two cutting edges and therefore increase the induced residual stress [44,45].

3.5.4. Cutting edge wear state

The cutting edge wear state is the most influential punching parameter. Comparing the local polarization curves independent of the material at a constant cutting clearance with each other, a significant increase of the punching affected area can be noticed. Using worn instead of sharp cutting edges results in a bigger initial cutting clearance.

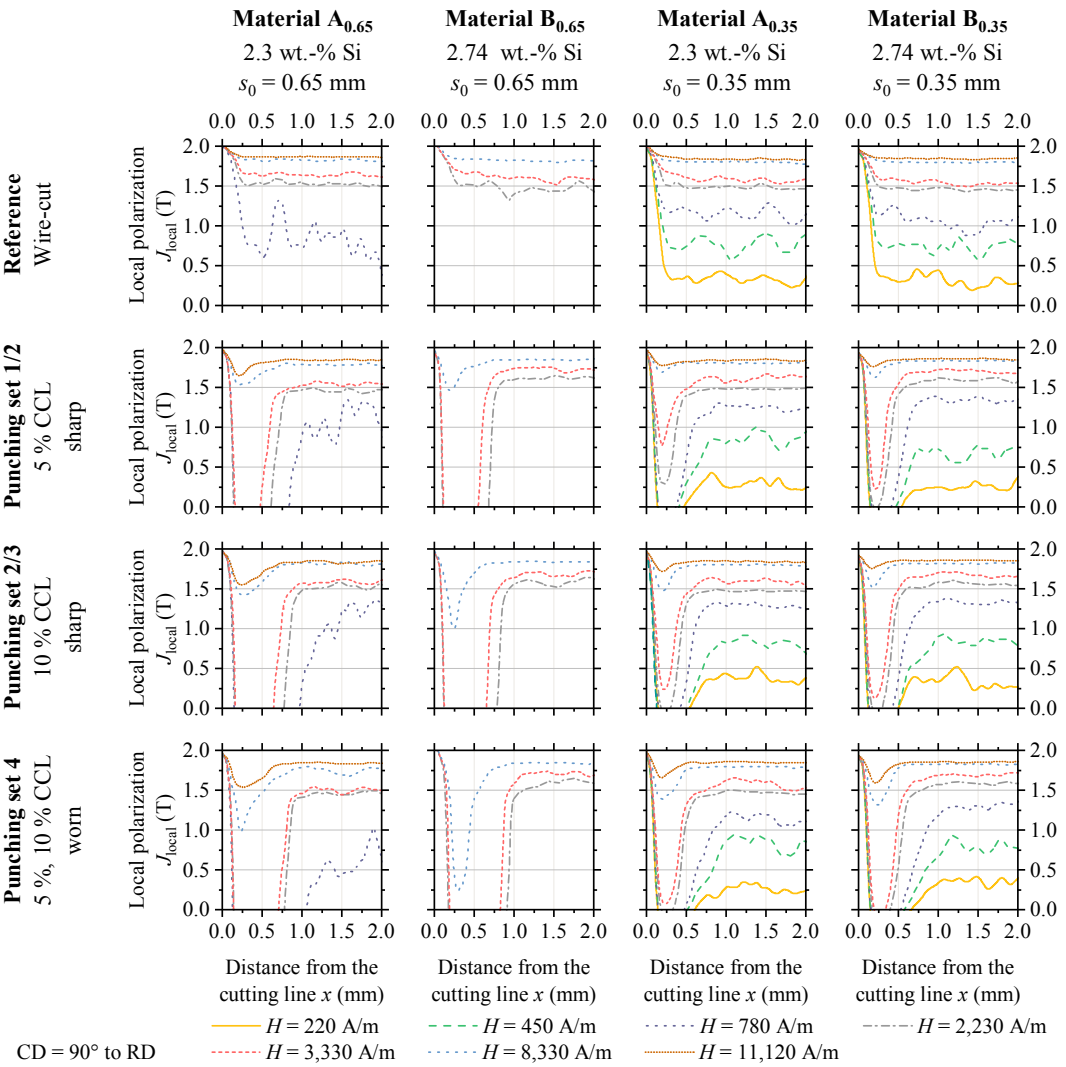

Fig. 12. Maximum local magnetic polarization J_{local} over the distance from the cutting line x for material $A_{0.65}$, $B_{0.65}$, $A_{0.35}$ and $B_{0.35}$ manufactured by wire-cutting and three different punching sets at different magnetic field strengths H.

The cutting edge wear state impact grows for an elevated sheet thickness and a higher silicon content.

3.6. Verification

To demonstrate the local magnetic investigation's trustworthiness a comparison with a global magnetic analysis of the cutting edge effect is carried out. In brief, this global analysis of the magnetic property deterioration is performed by varying the residual stress affected material volume inside the measurement volume of a single sheet tester by inserting specimens consisting of several smaller cut specimens. The method used to analyze the wire-cut and punched specimens is explained in detail in [12].

The global magnetic property deterioration is illustrated in Fig. 13 by displaying the first quadrant of the magnetic hysteresis loop measured at an excitation frequency of 50 Hz. Within the plots the impact of the above discussed cutting methods for material $A_{0.35}$ can be noticed by comparing hysteresis shearing (increase of coercivity H_C and reduction of remanence J_R) as well as the maximum magnetic field strength needed to reach the desired maximum polarization of each hysteresis to each other. Just like the local polarization distributions suggest, a similar behavior is indicated by the hysteresis, with the wire-cut specimens showing the least and the specimens punched with 10% CCL and worn cutting edges showing the greatest magnetic deterioration. A relative comparison of maximum magnetic field strengths of the punched with respect to the wire-cut specimens also demonstrates, that the punching effect has it's strongest influence for polarizations in between 1.0 T and 1.5 T just as predicted within the local investigation in Fig. 12.

4. Conclusion

The investigations of punched specimens using nGI allow for a non-destructive analysis of deteriorated local bulk magnetic properties for different manufacturing parameters. The functionality of the nGI setup combined with the newly designed magnetizing setup is ensured with a reproducibility and a specimen orientation measurement.

An analysis of the cutting line orientation shows that non-uniformly distributed magnetic material properties result from a crystallographic magnetic anisotropy. Thereby, varying sheet thicknesses and silicon contents affect the DFI contrast due to an alternating number of domains over the sheet thickness. Thinner electrical steels as well as higher silicon content reduce the number of scattered neutrons. As a consequence, higher mean DFI contrast values are measured.

Ex-situ measurements of the same specimens using an optional search coil at a frequency of 50 Hz enabled a correlation of dark field image contrast and global magnetic polarization. To determine the extent of the magnetically degraded area, measurements have been

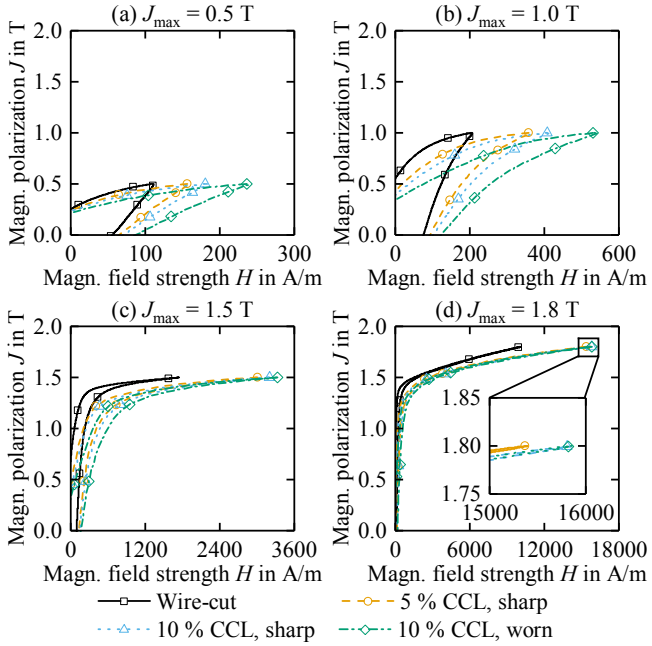

Fig. 13. Impact of wire-cutting and punching with different parameters on the magnetic hysteresis of material $A_{0.35}$ at varying maximum polarization levels and at 50 Hz.

carried out at different static magnetic field strengths.

Looking at the influence of the punching process on the local magnetic polarization, a significant influence of the processed material and the punching parameters has been observed. The thicker an electrical steel, the more stress is induced by the punching process, which results in an increased magnetic property deterioration. Local domain wall configurations of materials with a larger silicon content seem to be slightly more affected by the punching process itself and by a variation in the punching parameters. Changing the cutting clearance has a bigger influence when processing thicker electrical steels. The cutting edge wear state has a significant impact on the local magnetic polarization within the vicinity of the cutting line. Comparing these results with global magnetic property degradation analysis using a single-sheet tester setup presented in [12], a very good qualitative correspondence can be found.

In contrast to the extents of the local magnetic property deterioration due to cutting presented in Section 1, the investigations made using the nGI for the first time allow for an in situ, non-destructive investigation of electrical steel specimens manufactured with different process parameters. The results proove that not only the process parameters but also the current magnetic field strength has a large effect on the extent of the magnetically deteriorated material volume. It is also shown that outgoing from the cutting line the extent of the cutting edge effect reaches up to three times the blank thickness deep into the material. Nevertheless, like [18] noticed, the extent is far away from being just a constant value. By using the presented local polarization distributions material models to consider the cutting effect, as presented in [46], can be improved. This can be done by adding a variable cutting effect extent as well as a function that fits the local polarization distribution better than a hyperbolic approach.

5. Outlook

Due to the good correlation of the results acquired with nGI compared to single sheet test analysis of the punching influence in [12], an extended analysis for alternating magnetic fields is going to be carried out. This will help to understand the relationship between domain wall movement and induced residual stress.

Since the impact of punching on the local magnetic material properties is significant, other electrical steel grades will be investigated. Especially materials with a high silicon content and big grain size, like grain-oriented electrical steel that is used in transformers, will be examined.

The mapping database of each material presented in Fig. 11 will be extended by an additional stress axis. In doing so, stress-related magnetic domain structure variations can be taken into account when calculating the local polarization values from the DFI contrast signals. This will enable a more precise analysis of punching-related magnetic property degradations to be carried out.

Furthermore, the resulting local magnetic polarization curves will be implemented in the numerical magnetic field analysis of electrical drives. This allows the extent of punching related magnetic property deteriorations on the efficiency of electrical drives to be taken into account in more detail.

Acknowledgement

This work is funded by the Deutsche Forschungsgemeinschaft (DFG, German Research Foundation) 218259799, 255713208, 1487/31-1 and carried out in the research group project “FOR 1897 Low-Loss Electrical Steel for Energy-Efficient Electrical Drives” as well as in the priority program “SPP 2013 Focused Local Stress Imprint in Electrical Steel as Means of Improving the Energy Efficiency”.

This work is based upon experiments performed at the ANTARES instrument at Heinz Maier-Leibnitz Zentrum (MLZ), Garching, Germany.

Appendix A. Appendix

A.1. Reproducibility of measurement results

To prove the reproducibility of the acquired nGI data, one specimen out of material $A_{0.65}$ punched with PS 2 has been measured a second time. The cut specimen edges are aligned in 90° to rolling direction. In Fig. 14 the DFI contrast profile for the two measurements is plotted for a magnetic field strength of 3,333 A/m. Within the area next to both cutting lines, DFI contrast profiles are in excellent agreement with each other. A negligible fluctuation of the contrast values in the middle of the punched specimen can be noticed.

A.2. Investigation of the specimen orientation

The effect of the specimen orientation within the magnetization frame on the DFI contrast near the cutting surface is identified with two measurements of the same specimen. During the first measurement, the specimen’s burr is pointing towards the detector and, during the second measurement, the burr points away from the detector. The specimen out of material $A_{0.65}$ is punched using PS 4 with a cutting line orientation perpendicular to rolling direction. Fig. 15 displays the DFI contrast profiles of both measurements. It is obvious that the orientation of the specimen has no influence on the DFI contrast profile next to the cutting surfaces. This confirms that there are no cross talk effects on the edges of the sample. The investigation shows that the DFI contrast profile only depends on the local domain wall configuration and not on the geometrical characteristics of the specimen.

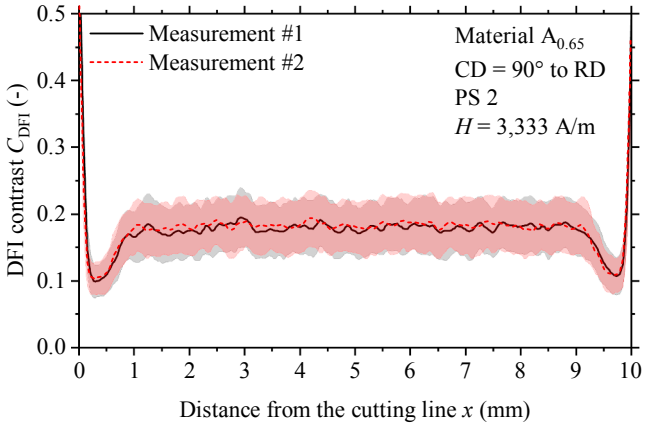

Fig. 14. DFI contrast profiles for a specimen out of material $A_{0.65}$ punched with PS 2 in 90° to rolling direction at a magnetic field strength of 3,333 A/m.

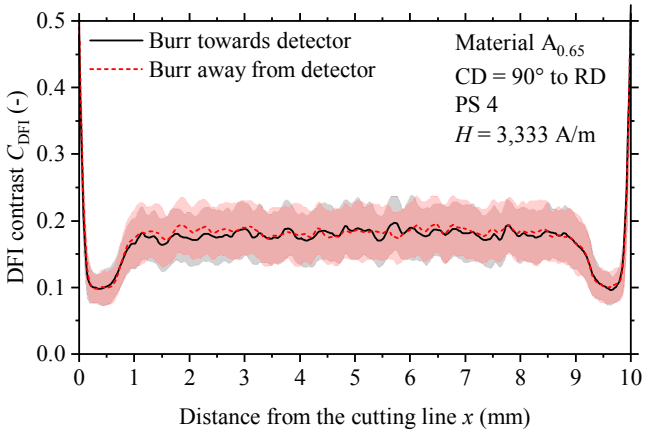

Fig. 15. Effect of the specimen orientation on the DFI contrast profile of material $A_{0.65}$ punched with PS 4 at a magnetic field strength of 3,333 A/m.

References

[1] Y. Kurosaki, H. Mogi, H. Fujii, T. Kubota, M. Shiozaki, Importance of punching and workability in non-oriented electrical steel sheets, J. Magn. Magn. Mater. 320 (20) (2008) 2474–2480, https://doi.org/10.1016/j.jmmm.2008.04.073.

[2] A. Moses, Effects of applied stress on the magnetic properties of high permeability silicon-iron, IEEE Trans. Magn. 15 (6) (1979) 1575–1579, https://doi.org/10.1109/TMAG.1979.1060392.

[3] R.G. Hancock, The effects of stress relief annealing on the magnetic properties of cut laminations and assembled cores produced from nonoriented electrical steel, J. Magn. Magn. Mater. 19 (1–3) (1980) 65–68, https://doi.org/10.1016/0304-8853(80)90555-7.

[4] K.H. Schmidt, Influence of punching on the magnetic properties of electric steel with 1% silicon: Der einfluss des stanzens auf die magnetischen eigenschaften von elektroblech mit 1% silizium, J. Magn. Magn. Mater. 2 (1–3) (1975) 136–150, https://doi.org/10.1016/0304-8853(75)90116-X.

[5] H.A. Weiss, N. Leuning, S. Steentjes, K. Hameyer, T. Andorfer, S. Jenner, W. Volk, Influence of shear cutting parameters on the electromagnetic properties of non-oriented electrical steel sheets, J. Magn. Magn. Mater. 421 (2017) 250–259, https://doi.org/10.1016/j.jmmm.2016.08.002.

[6] R.M. Bozorth, Ferromagnetism, IEEE Press, Piscataway, NJ, 1978.

[7] K. Ali, K. Atallah, D. Howe, Prediction of mechanical stress effects on the iron loss in electrical machines, J. Appl. Phys. 81 (8) (1997) 4119–4121, https://doi.org/10.1063/1.365099.

[8] H. Naumoski, A. Maucher, U. Herr, Investigation of the influence of global stresses and strains on the magnetic properties of electrical steels with varying alloying content and grain size, in: 2015 5th International Electric Drives Production Conference (EDPC), pp. 1–8. doi:10.1109/EDPC.2015.7323206.

[9] N. Leuning, S. Steentjes, M. Schulte, W. Bleck, K. Hameyer, Effect of elastic and plastic tensile mechanical loading on the magnetic properties of ngo electrical steel, J. Magn. Magn. Mater. 417 (2016) 42–48, https://doi.org/10.1016/j.jmmm.2016.05.049.

[10] P. Rasilo, U. Aydin, T.P. Holopainen, A. Arkkio, Analysis of iron losses on the cutting edges of induction motor core laminations, in: 2016 XXII International Conference on Electrical Machines (ICEM), pp. 1312–1317. doi:10.1109/ICELMACH.2016.7732694.

[11] S. Elfgen, S. Steentjes, S. Bohmer, D. Franck, K. Hameyer, Continuous local material model for cut edge effects in soft magnetic materials, IEEE Trans. Magn. 52 (5) (2016) 1–4, https://doi.org/10.1109/TMAG.2015.2511451.

[12] H.A. Weiss, P. Trober, R. Golle, S. Steentjes, N. Leuning, S. Elfgen, K. Hameyer, W. Volk, Impact of punching parameter variations on magnetic properties of non-grain oriented electrical steel, 2018. pp. 1–1. doi:10.1109/TIA.2018.2853133.

[13] U. Aydin, P. Rasilo, F. Martin, D. Singh, L. Daniel, A. Belahcen, R. Kouhia, A. Arkkio, Modeling the effect of multiaxial stress on magnetic hysteresis of electrical steel sheets: a comparison, IEEE Trans. Magn. 53 (6) (2017) 1–4, https://doi.org/10.1109/TMAG.2017.2658676.

[14] K. Yamazaki, H. Mukaiyama, L. Daniel, Effects of multi-axial mechanical stress on loss characteristics of electrical steel sheets and interior permanent magnet machines, IEEE Trans. Magn. (2017) 1–4, https://doi.org/10.1109/TMAG.2017.2757531.

[15] M. Bali, H.D. Gersem, A. Muetze, Determination of original nondegraded and fully degraded magnetic properties of material subjected to mechanical cutting, IEEE Trans. Ind. Appl. 52 (3) (2016) 2297–2305, https://doi.org/10.1109/TIA.2016.2532288.

[16] M. Hofmann, H. Naumoski, U. Herr, H.-G. Herzog, Magnetic properties of electrical steel sheets in respect of cutting: micromagnetic analysis and macromagnetic modeling, IEEE Trans. Magn. 52 (2) (2016) 1–14, https://doi.org/10.1109/TMAG.2015.2484280.

[17] T.P. Holopainen, P. Rasilo, A. Arkkio, Identification of magnetic properties for cutting edge of electrical steel sheets, IEEE Trans. Ind. Appl. 53 (2) (2017) 1049–1053, https://doi.org/10.1109/TIA.2016.2638405.

[18] T. Nakata, M. Nakano, K. Kawahara, Effects of stress due to cutting on magnetic characteristics of silicon steel, IEEE Transl. J. Magn. Jpn. 7 (6) (1992) 453–457, https://doi.org/10.1109/TJMJ.1992.4565422.

[19] R. Rygal, A. Moses, N. Derebasi, J. Schneider, A. Schoppa, Influence of cutting stress on magnetic field and flux density distribution in non-oriented electrical steels, J. Magn. Magn. Mater. 215–216 (2000) 687–689, https://doi.org/10.1016/S0304-8853(00)00259-6.

[20] H. Naumoski, B. Riedmüller, A. Minkow, U. Herr, Investigation of the influence of different cutting procedures on the global and local magnetic properties of non-oriented electrical steel, J. Magn. Magn. Mater. 392 (2015) 126–133, https://doi.

org/10.1016/j.jmmm.2015.05.031.
[21] H. Cao, L. Hao, J. Yi, X. Zhang, Z. Luo, S. Chen, R. Li, The influence of punching process on residual stress and magnetic domain structure of non-oriented silicon steel, J. Magn. Magn. Mater. 406 (2016) 42–47, https://doi.org/10.1016/j.jmmm.2015.12.098.
[22] Y. Zaizen, T. Omura, M. Fukumura, K. Senda, H. Toda, Evaluation of stress distribution due to shearing in non-oriented electrical steel by using synchrotron radiation, AIP Adv. 6 (5) (2016) 055926, https://doi.org/10.1063/1.4944342.
[23] C. Grünzweig, C. David, O. Bunk, M. Dierolf, G. Frei, G. Kühne, R. Schäfer, S. Pofahl, H.M.R. Rønnow, F. Pfeiffer, Bulk magnetic domain structures visualized by neutron dark-field imaging, Appl. Phys. Lett. 93 (11) (2008) 112504, https://doi.org/10.1063/1.2975848.
[24] C. Grünzweig, C. David, O. Bunk, J. Kohlbrecher, E. Lehmann, Y.W. Lai, R. Schäfer, S. Roth, P. Lejcek, J. Kopecek, F. Pfeiffer, Visualizing the propagation of volume magnetization in bulk ferromagnetic materials by neutron grating interferometry (invited), J. Appl. Phys. 107 (9) (2010) 09D308, https://doi.org/10.1063/1.3365373.
[25] R. Siebert, A. Wetzig, E. Beyer, B. Betz, C. Grunzweig, E. Lehmann, Localized investigation of magnetic bulk property deterioration of electrical steel: analysing magnetic property drop thorough mechanical and laser cutting of electrical steel laminations using neutron grating interferometry, in: 2013 3rd International Electric Drives Production Conference (EDPC), pp. 1–5. doi:10.1109/EDPC.2013.6689726.
[26] B. Betz, P. Rauscher, R. Siebert, R. Schaefer, A. Kaestner, H. van Swygenhoven, E. Lehmann, C. Grünzweig, Visualization of bulk magnetic properties by neutron grating interferometry, Phys. Procedia 69 (2015) 399–403, https://doi.org/10.1016/j.phpro.2015.07.056.
[27] R. Siebert, J. Schneider, E. Beyer, Laser cutting and mechanical cutting of electrical steels and its effect on the magnetic properties, IEEE Trans. Magn. 50 (4) (2014) 1–4, https://doi.org/10.1109/TMAG.2013.2285256.
[28] B. Betz, P. Rauscher, R.P. Harti, R. Schäfer, H. van Swygenhoven, A. Kaestner, J. Hovind, E. Lehmann, C. Grünzweig, In-situ visualization of stress-dependent bulk magnetic domain formation by neutron grating interferometry, Appl. Phys. Lett. 108 (1) (2016) 012405, https://doi.org/10.1063/1.4939196.
[29] I. Manke, N. Kardjilov, R. Schäfer, A. Hilger, M. Strobl, M. Dawson, C. Grünzweig, G. Behr, M. Hentschel, C. David, A. Kupsch, A. Lange, J. Banhart, Three-dimensional imaging of magnetic domains, Nat. Commun. 1 (2010) 125, https://doi.org/10.1038/ncomms1125.
[30] C. Grünzweig, J. Kopecek, B. Betz, A. Kaestner, K. Jefimovs, J. Kohlbrecher, U. Gasser, O. Bunk, C. David, E. Lehmann, T. Donath, F. Pfeiffer, Quantification of the neutron dark-field imaging signal in grating interferometry, Phys. Rev. B 88 (12) (2013) 47, https://doi.org/10.1103/PhysRevB.88.125104.
[31] E. Lau, Interference phenomenon on double gratings: Beugungserscheinungen an doppelrastern, Ann. Phys. 437 (7–8) (1948) 417–423, https://doi.org/10.1002/andp.19484370709.
[32] T. Reimann, Vortex matter beyond sans (Ph.D. thesis), Technische Universität München, München, 2017.
[33] A. Hipp, M. Willner, J. Herzen, S. Auweter, M. Chabior, J. Meiser, K. Achterhold, J. Mohr, F. Pfeiffer, Energy-resolved visibility analysis of grating interferometers operated at polychromatic X-ray sources, Opt. Express 22 (25) (2014) 30394–30409, https://doi.org/10.1364/OE.22.030394.
[34] C. Grünzweig, G. Frei, E. Lehmann, G. Kühne, C. David, Highly absorbing gadolinium test device to characterize the performance of neutron imaging detector systems, Rev. Scientific Instrum. 78 (5) (2007) 053708, https://doi.org/10.1063/1.2736892.
[35] T. Reimann, S. Mühlbauer, M. Horisberger, B. Betz, P. Böni, M. Schulz, The new neutron grating interferometer at the antares beamline: design, principles and applications, J. Appl. Crystallogr. 49 (5) (2016) 1488–1500, https://doi.org/10.1107/S1600576716011080.
[36] M. Chabior, Contributions to the characterization of grating-based x-ray phase-contrast imaging (Dissertation), Technische Universität Dresden, Dresden, 2011 URL:http://nbn-resolving.de/urn:nbn:de:bsz:14-qucosa-81705.
[37] S. Marathe, L. Assoufid, X. Xiao, K. Ham, W.W. Johnson, L.G. Butler, Improved algorithm for processing grating-based phase contrast interferometry image sets, Rev. Sci. Instrum. 85 (1) (2014) 013704, https://doi.org/10.1063/1.4861199.
[38] H. Strothmann, O. Schärpf, Measurement concerning the refraction behaviour of neutrons in bloch walls by means of a double crystal arrangement, J. Magn. Magn. Mater. 9 (1) (1978) 257–260, https://doi.org/10.1016/0304-8853(78)90065-3.
[39] M. Schulz, B. Schillinger, Antares: cold neutron radiography and tomography facility, J. Large-Scale Res. Facilities 1. doi:10.17815/jlsrf-1-42.
[40] E. Calzada, F. Gruenauer, M. Mühlbauer, B. Schillinger, M. Schulz, New design for the antares-ii facility for neutron imaging at FRM II, Nucl. Instrum. Methods Phys. Res. Sect. A 605 (1–2) (2009) 50–53, https://doi.org/10.1016/j.nima.2009.01.192.
[41] M. Shiozaki, Y. Kurosaki, The effects of grain size on the magnetic properties of nonoriented electrical steel sheets, J. Mater. Eng. 11 (1) (1989) 37–43, https://doi.org/10.1007/BF02833752.
[42] T. Kals, R. Eckstein, Miniaturization in sheet metal working, J. Mater. Process. Technol. 103 (1) (2000) 95–101, https://doi.org/10.1016/S0924-0136(00)00391-5.
[43] J. Xu, B. Guo, C. Wang, D. Shan, Blanking clearance and grain size effects on micro deformation behavior and fracture in micro-blanking of brass foil, Int. J. Mach. Tools Manuf. 60 (2012) 27–34, https://doi.org/10.1016/j.ijmachtools.2012.04.001.
[44] M. Sasada, T. Togashi, Measurement of rollover in double-sided shearing using image processing and influence of clearance, Procedia Eng. 81 (2014) 1139–1144, https://doi.org/10.1016/j.proeng.2014.10.248.
[45] Ł. Bohdal, A. Kułakowska, R. Patyk, M. Kulakowski, Numerical investigations of the effect of process parameters on residual stresses, strains and quality of final product in blanking using SPH method, Mater. Sci. Forum 862 (2016) 238–245, https://doi.org/10.4028/www.scientific.net/MSF.862.238.
[46] L. Vandenbossche, S. Jacobs, F. Henrotte, K. Hameyer, Impact of cut edges on magnetization curves and iron losses in e-machines for automotive traction, World Electric Vehicle J. 4 (3) (2010) 587–596, https://doi.org/10.3390/wevj4030587.